Heliyon

Received:
9 November 2018
Revised:
24 February 2019
Accepted:
25 March 2019

Cite as: S. N. Pleskova, R. N. Kriukov, E. N. Gorshkova, A. V. Boryakov. Characteristics of quantum dots phagocytosis by neutrophil granulocytes. Heliyon 5 (2019) e01439. doi: 10.1016/j.heliyon.2019.e01439

Characteristics of quantum dots phagocytosis by neutrophil granulocytes

S. N. Pleskova [a,b,*], **R. N. Kriukov** [a], **E. N. Gorshkova** [a], **A. V. Boryakov** [a]

[a] *Lobachevsky State University of Nizhny Novgorod, Nizhny Novgorod, 603950, Russia*

[b] *R.E. Alekseev Nizhny Novgorod Technical State University, Nizhny Novgorod, 603950, Russia*

[*] Corresponding author.

E-mail address: pleskova@mail.ru (S.N. Pleskova).

Abstract

This article describes the main morphological and biochemical features of neutrophil granulocytes in the process of phagocytosis of two types of quantum dots (CdSe/ZnS-MPA and CdSe/CdSeZnS/ZnS-PTVP). This study is the first to observe the transfer of large aggregates of quantum dots through neutrophils. During this process the cells demonstrate high chemotactic activity. Furthermore, neutrophil pseudopodia underwent alterations during the early stages of phagocytosis. The findings demonstrated that the biochemical profile of neutrophils is practically identical after phagocytosis of both types of quantum dots, but differs significantly from neutrophil metabolism after bacterial phagocytosis.

Keywords: Biochemistry, Biophysics, Cell biology, Physiology

1. Introduction

Phagocytosis is a fundamental process of cells capturing foreign particles (Uribe-Querol and Rosales, 2017). For professional phagocytes, this is an effective mechanism for countering microbial invasion, clearance of the organism, elimination of pathogens, and restoration of homeostasis (Rabinovitch, 1995; Fine et al., 2017). Neutrophils can capture objects larger than 0.5 μm. The kinetics of the bacterial phagocytosis process is well known and thoroughly described in numerous studies

https://doi.org/10.1016/j.heliyon.2019.e01439

(Beste et al., 2015; Sakai et al., 2012; Nüsse, 2011; Nordenfelt and Tapper, 2011; Oberdörster et al., 2007).

However, professional phagocytes (neutrophils and macrophages) have to deal with objects that they did not have a long evolutionary contact with. Nanomaterials (i.e. objects smaller than 10^{-9} m according to X, Y or Z axes, or all three axes) can serve as an example of such objects, in particular those with «engineering nanoparticles» (Oberdörster et al., 2007). In our previous study, it was proved that nanoparticles can also be engulfed by neutrophil granulocytes using the mechanism of phagocytosis (Pleskova et al., 2018b). Nanoparticles facilitate this process by forming aggregates of different sizes when interacting with cells, primarily due to the formation of a «protein crown» and lipids that surround the nanoparticles both as a result of interaction with cell membranes and after cell destruction. Macrophages also demonstrated the ability to phagocytize nanomaterials (Gatto et al., 2017). In addition, it was established that preincubation with nanoparticles primes neutrophils and they strengthen their phagocytic activity against other objects, including opsonized red blood cells of sheep and fluorescent latex beads according to the Syk-dependent mechanism (Babin et al., 2015).

In this study, we observed morphological features of phagocytosis of two types of quantum dots (QDs), CdSe/ZnS-MPA and CdSe/CdZnS/ZnS-PTVP, by neutrophil granulocytes and estimated the change in the biochemical profile of cells as a result of this process. QDs are fluorescent semiconductor nanocrystals consisting of atomic elements of II–IV or III–V groups of the *Mendeleev periodic* table with the size less than the Bohr exciton radius for this material (Yashin et al., 2007; Guo, Tan, 2009). They have the properties of controllable photoluminescence due to the effect of dimensional quantization (Musihin et al., 2012). This effect is very important for biology and medicine, since it allows the labeling of cellular elements in biology and the diagnosis of certain diseases in medicine. The existing organic fluorophors are of limited use owing to such restrictions as fast photobleaching, wide range of emission and necessity for constant selection of a suitable source of excitement. QDs do not have these disadvantages. QDs are used in classical biology for studying transport mechanisms in a cell (Belyaeva et al., 2009), including endocytosis (Lidke et al., 2004), functional heterogeneity of cells (Pleskova et al., 2009), diffusion movements of membrane transport proteins (Crane et al., 2009), intracellular organelle marking (Hanaki et al., 2003). In medicine, QDs are used for contrasting of blood and lymph vessels (including microvessels) (Lim et al., 2003), but first of all for multiplex molecular diagnostics and visualization *in vivo* (Wu et al., 2002; Gao et al., 2004; Kim et al., 2004; Rhyner et al., 2006; Xing et al., 2007).

The overwhelming majority of studies of QD phagocytosis have been done on macrophages (Liu et al., 2013; Xu et al., 2018; Xie et al., 2019). This is important, as in case of using QDs for theranostics (therapy + diagnostics), they may not reach the

https://doi.org/10.1016/j.heliyon.2019.e01439

target organ in therapeutic and/or diagnostic concentration as they are phagocytized by macrophages en masse.

At the same time, another class of phagocytes can be present in the tissue alongside macrophages. These are neutrophils, which migrate into the tissue in case of inflammation. In addition, regardless of the mechanism of QDs penetration into the human body, they are always found in blood. The main fraction of blood leukocytes are neutrophils, which can bind and phagocytose QDs. Therefore, it is important to understand not only how effective the process of QDs phagocytosis by neutrophil granulocytes is, but also what kind of cell changes this process causes.

2. Materials and methods

2.1. QDs were acquired from «Nanotech-Dubna» (Russia). Two kinds of QDs were used:

(i) CdSe core with ZnS shell coated by mercaptopropionic acid (CdSe/ZnS - MPA), round form, emission peak wavelength 620 nm, averaged diameter 10 nm (according to the manufacturer's specifications), 18.7 $\pm$ 2.4 nm with hydrodynamic diameter (according dynamic light scattering (DLS) data), height $-$ 9.03 $\pm$ 1.17 nm (according the atomic force microscopy (AFM) data), ζ-potential (-18.2 $\pm$ 0.8) mV;

(ii) CdSe/CdZnS core with ZnS shell coated by polyvinylpyrrolidone heterobifunctional polymer with amber anhydride and thiol groups (CdSe/CdSeZnS/ZnS-PTVP), round form, emission peak wavelength 588 nm, averaged diameter 18 nm (according to the manufacturer's specifications), 21.0 $\pm$ 0.1 nm with hydrodynamic diameter (according DLS data) height $-$ 17.57 $\pm$ 2.03 nm (according the AFM data), ζ-potential (-15.3 $\pm$ 1.0) mV.

In all experiments, we used QDs in CL_{50}, which were obtained earlier (Pleskova et al., 2018b) and which were 0.025 mg/ml for CdSe/ZnS-MPA and 0.04 mg/ml for CdSe/CdSeZnS/ZnS-PTVP, respectively.

2.2. Neutrophils

Venous blood was obtained from healthy volunteers and stabilized by 5 U/ml of heparin. All volunteers participated by written, informed consent, endorsed by the ethical committee of Lobachevsky State University of Nizhny Novgorod. Research approved by the ethical committee of Lobachevsky State University of Nizhny Novgorod (№ 9 from 07.17.2017) The neutrophils were isolated on discontinuous Ficoll-Urografin gradients essentially as described (Aguado et al., 1980). Purity of

https://doi.org/10.1016/j.heliyon.2019.e01439

neutrophils isolated by this method reaches 95.57 ± 1.86%. The neutrophil fractions were rinsed twice (200g, 3 min), resuspension in phosphate buffered saline (PBS), and used in a final concentration of $1 \cdot 10^6$ cells/ml.

2.3. Flow cytometry

Neutrophils were treated with CdSe/ZnS-MPA (final concentration 0.025 mg/ml) or CdSe/CdZnS/ZnS-PTVP (final concentration 0.04 mg/ml) (37 °C, 5% CO_2). After that, the cells were incubated in the dark for 25, 35, 45, 55, 65, and 75 min. After the incubation, to destroy erythrocytes red blood cell lysis buffer (BD Bioscience, USA) was added and incubated (10 min). The cell suspension was centrifuged for 7 min at 500 g, rinsed and resuspended in 1 ml of PBS. This process was then repeated and the cells were resuspended in 300 μl PBS.

Using the light filter with the transmission band suitable for the emission of both kinds of QDs (610/20 nm), the geometric mean fluorescent intensity was analyzed immediately at each time point using flow cytometry (Cytoflex S, Beckman Coulter, USA).

In order to detect differences in binding to the cell surface and internalization of QDs by neutrophils, there were two versions of the test: (i) at 37 °C (internalization of QDs) and (ii) at 4 °C (nonspecific binding of QDs to the cell surface).

2.4. Methods of scanning electron microscopy (SEM) and X-ray microanalysis (EDXMA)

The cells were transferred to a gold/aluminum substrate and fixed with glutaraldehyde (2.5%, 20 min, 24 °C), then washed three times. The tests were carried out using a scanning electron microscope JSM-IT300LV (JEOL, Japan) in high vacuum mode with an accelerating voltage of 20 kV, the electron beam diameter reached 5 nm. To conduct EDXMA, the X-Max^N 20 energy dispersing detector (Oxford Instruments, UK) was used. The EDXMA mode was used to create maps (scanning raster 256 × 256 or 512 × 512 pixels) of element distribution over the surface and determine the composition at certain points of local analysis. An entire map was produced within the period of around 1 h. Each individual scanning point accumulated its own spectrum. The beam current did not exceed 0.5 nA to minimize the effect on the cells.

2.5. Atomic force microscopy

To study fixed preparations, we used a sample nearly identical to the SEM method with glass slides serving as a substrate. The cells were scanned in a semi-contact mode in the air by Ntegra Spectra system (NT-MDT, Russia). To process the scanning results, we used the Topometrix software package (USA). The test involved the

https://doi.org/10.1016/j.heliyon.2019.e01439

use of DNP probes (Bruker, USA) with a tip radius of 20 nm, front angle of 15°, resonance frequency 65 kHz, spring constant of 0.35 N/m.

The real-time AFM studies of native cells were carried out using the method described in a previous study (Pleskova et al., 2005). The morphology was studied in the vital state. The test involved the use of MLCT probes (Bruker, USA) with the tip radius of 20 nm, front angle 15°, and resonance frequency in fluid 14 kHz. After 30 min of control scanning, the QDs were added into the Petri dish in CL_{50} concentration (final concentration 0.025 mg/ml and 0.04 mg/ml for CdSe/ZnS-MPA and CdSe/CdZnS/ZnS-PTVP respectively).

2.6. Laser scanning confocal microscopy of the living cells

2 ml of neutrophil suspension ($1 \cdot 10^6$ cells/ml) were added to a 45 mm Petri dish. After the incubation during 20 min, the cells were washed twice with Hank's balanced salt solution (HBSS). The measurements were carried out inside a closed chamber by Zeiss Axiovert 200M LSM 510 META, Germany. There were no QDs in the control series of samples. For other experiments, QDs (in the final concentration of 0.1 mg/ml) were added to the cells.

To monitor live imaging of the QD phagocytosis by the cells, we used confocal laser scanning microscopy during 3 h at the frame rate of 7.5 frames min^{-1} at $\times 100$ magnification. The QDs were excited with an argon laser (488 nm, 30 mV), the QD emission was registered within the emission wavelength band from 543 to 627 nm.

2.7. Nitroblue tetrazolium test

The activity of neutrophil NADPH-oxidase was evaluated using (Mayansky and Pikusa, 1993): nitroblue tetrazolium (NBT) reduction reaction (ThermoFisher scientific, USA). The number of NBT-positive cells (containing insoluble diformazan granules) before incubation with QDs (control) and after incubation with CdSe/ZnS-MPA or CdSe/CdZnS/ZnS-PTVP (experiments) was evaluated. The number of NBT-positive cells was used to assess spontaneous cell reaction in the absence of additional stimulation; the stimulated reaction was estimated after the implementation of a respiratory burst caused by opsonized zymosan. The activation index (AI) of neutrophil granulocytes was calculated according to the formula:

AI = NBT-positive cells in the stimulated test/NBT-positive cells in the spontaneous test,

and functional reserve of neutrophil granulocytes (NFR):

NFR = NBT-positive cells in the stimulated test − NBT-positive cells in the spontaneous test.

https://doi.org/10.1016/j.heliyon.2019.e01439

2.8. Myeloperoxidase activity

Myeloperoxidase activity (MPO) was determined according to the Graham-Knoll method (Bazarny et al., 2012). After incubation in silicone tubes with QDs, the cells were applied to the glass surface, fixed with a 10% alcohol/formalin solution and stained with an alcohol solution of ortho-tolidine (Diakhim-Cytostain-MPO, NPF « Abris+», Russia). The degree of azurophilic granules coloration of 100 cells was evaluated prior to incubation with QDs (control) and after incubation (experiment) applying the Astaldi principle (Astaldi and Verga, 1957). To get a quantitative evaluation of the results, an average cytochemical coefficient (ACC) was calculated according to (Kaplow, 1995):

$$ACC = (0 \cdot a + 1 \cdot b + 2 \cdot c + 3 \cdot d) / 100,$$

where a is the number of neutrophils without diformazan granules; b, c, d are the number of neutrophils with stained cytoplasm. Numbers indicate the degree of cytoplasm staining: 0 − without diformazan granules; 1 − slight cytoplasm staining; 2 − medium intensity staining; 3 − intensely colored cytoplasm.

2.9. Lysosomal-cationic test

Cationic proteins (CP) content was determined using the Pigarevsky method (Pigarevskiy, 1988). After application of the cells to the glass, they were fixed by drying, then the granules were stained with a 0.1% fast green solution (20 min, 25 °C) on a Tris-HCl buffer with methanol. They were washed twice with distilled water; the nuclei were stained with a 0.25% aqueous solution of Azure A. After that, the ACC was evaluated as described in 2.8.

2.10. Statistical analysis

The study used Origin 7.0 Server Package for statistical analysis. We determined, whether the values belonged to the normal attribution using the Mann-Whitney test. Since most of the values were characterized as abnormal distributions, Wilcoxon test was used for estimating the significant difference between two values (control end experiment).

3. Results and discussion

3.1. Study of quantum dots phagocytosis using flow cytometry

Binding and internalization of QDs were evaluated by flow cytometry. The results of the study are shown in Fig. 1.

Phagocytosis is an active metabolic process, which stops at low temperatures, while non-specific binding of QDs on the cell's membranes occurs at low temperatures, as

https://doi.org/10.1016/j.heliyon.2019.e01439

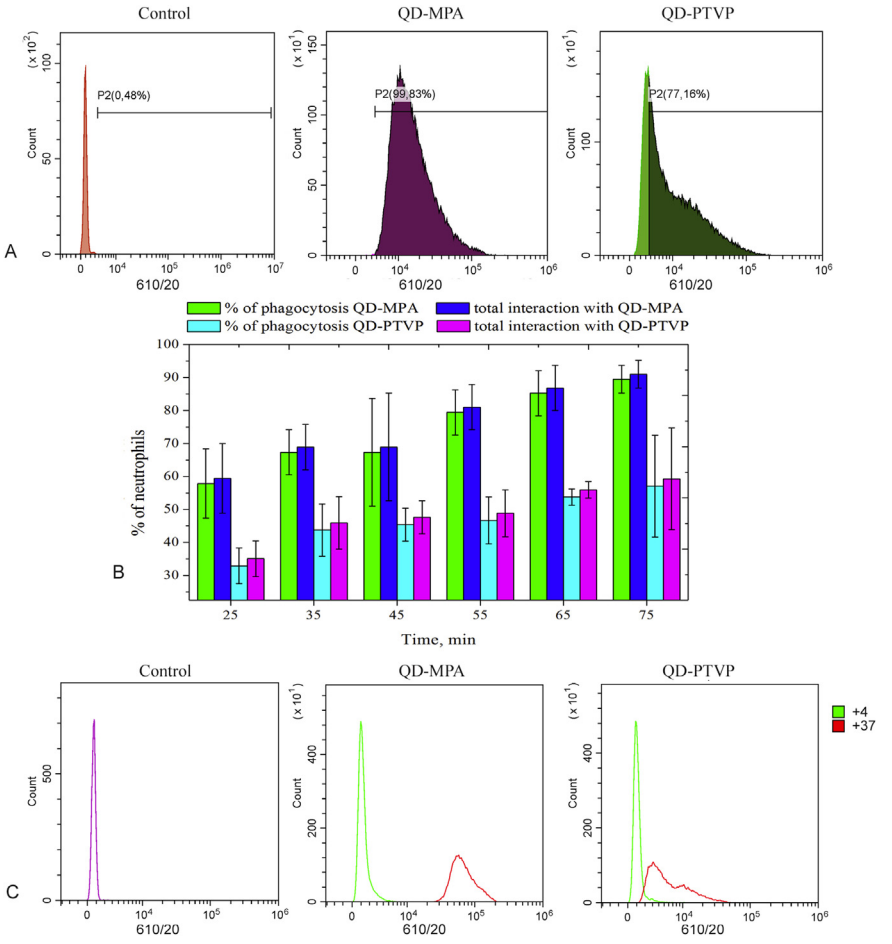

Fig. 1. Neutrophils interaction with QDs. A. Representative flow cytometry histograms depicting the accumulation of QDs in neutrophils. B. Diagram confirming that phagocytosis makes the main contribution to the accumulation of QDs by neutrophils. C. Representative flow cytometry histograms demonstrating the number of cells that nonspecific adsorbed QDs (dotted grey line) and the number of neutrophils that internalized QDs (solid black line).

this process is not energy-dependent. The results of the comparison between only binding (at 4 °C) and general interaction (i.e. binding and internalization at 37 °C) prove the phagocytosis of both types of QDs by neutrophil granulocytes (Fig. 1), but the presence of complex polymer structures on the surface of QDs (CdSe/CdZnS/ZnS-PTVP) significantly reduces both phagocytosis and surface binding to membranes of neutrophils. Most likely, the reason lies in the steric features of long polymer structures that hamper the initial contact of neutrophil with QDs. This is consistent with the results of Abdelmonem et al. (2015), which showed that ZnO nanoparticles without a polymer coating are more prone to aggregation and are absorbed more actively than well-dispersed particles with a polymer coating. Phagocytosis of QDs was also proved by us earlier based on the overlap of the profiles of colocalization of LysoTracker and the QDs signal (Pleskova et al., 2018b). This study showed that QDs are found exclusively inside of neutrophil granulocytes

https://doi.org/10.1016/j.heliyon.2019.e01439

phagolysosomes, which is direct evidence of the phagocytosis process. Here we also provide evidence of QDs phagocytosis by high-resolution microscopy (SEM and AFM) and examine the features of this process with regard to nanomaterials to identify the main difference with the classical phagocytosis of bacteria.

3.2. Characteristics of the QDs phagocytosis by the SEM method

Fig. 2 demonstrates the results of the study of the QDs phagocytosis by neutrophil granulocytes.

In control, the neutrophil granulocyte is spread out on the surface of the substrate, the nucleus and granules are well visualized, the cell is not altered (Fig. 2a). After 15 min of incubation with CdSe/ZnS-MPA, we identified the cells forming developed pseudopodia to capture QDs (Fig. 2b). However, these pseudopodia are distinctly different from similar structures formed during the phagocytosis of bacteria. In particular, in the process of opsonized *S. aureus* 2879M phagocytosis, neutrophils form long, pronounced, well-branched pseudopodia (Pleskova et al., 2018a) without features of damage or destruction (Fig. 3). In the case of interaction with QDs, the pseudopodia are shorter, straight, but the main feature of their differences from the classic structures are the sections of melting at the ends, which were also recorded by AFM (p. 3.4, Fig. 5a, b). Another feature is the presence of disseminated CdSe/ZnS-MPA aggregates in the cell cytoplasm 15 min after the start of the incubation of cells with QDs (Fig. 2b), whereas after 30 min large, structured QDs

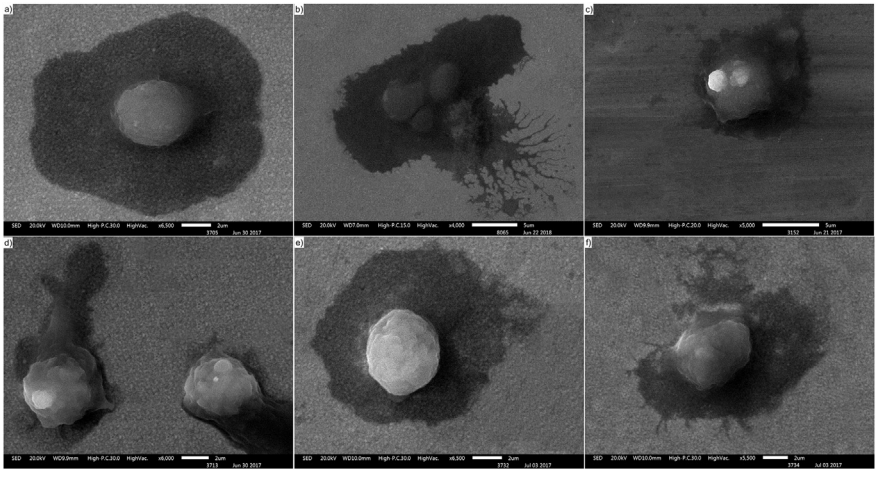

Fig. 2. Neutrophils were studied by SEM on a substrate – gold (Au/GaAs): (a) control (non-treated neutrophil); (b) formation of «melted » pseudopodia with neutrophil granulocytes 15 min after interaction with CdSe/ZnS-MPA; (c) cell polarization and formation of large QD aggregates in the nucleus area 30 min after interaction with CdSe/ZnS-MPA; (d) cell polarization and formation of large QD aggregates in the nucleus area 15 min after interaction with CdSe/CdZnS/ZnS-PTVP; (e), (f) areas of «thinning of the cytoplasmic region of the membrane» and partial destruction of the cells 30 min after interaction with CdSe/CdZnS/ZnS-PTVP.

https://doi.org/10.1016/j.heliyon.2019.e01439

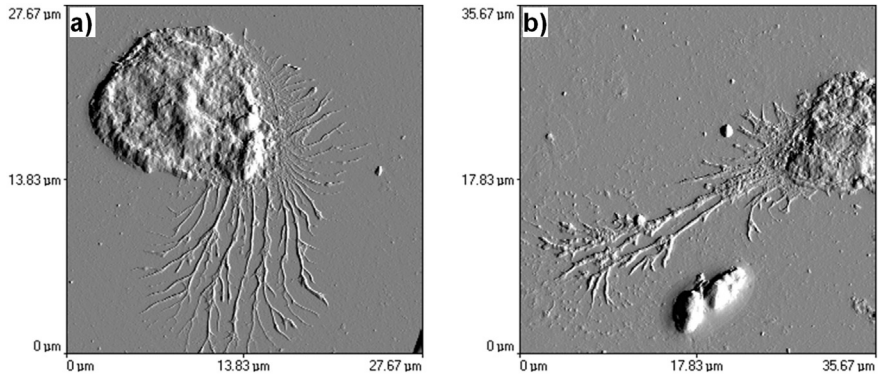

Fig. 3. Phagocytosis of opsonized *S. aureus* by neutrophil granulocytes: cells form long, branched, well developed, undamaged pseudopodia. Smears fixed with methanol and studied by AFM: (a) $5 \cdot 10^6$ bacteria/ml, (b) $1 \cdot 10^9$ bacteria/ml.

aggregates form in the nucleus area (Fig. 2c). According to the results of confocal microscopy (in Appendix), it was also revealed that the neutrophils first captured small aggregates of QDs, then they significantly enlarge these aggregates and move them to the nucleus areas.

After 15 min of neutrophil incubation with CdSe/CdZnS/ZnS-PTVP, a marked polarization of the cells is observed, and in a number of cells the formation of large aggregates of QDs in the nucleus areas can already be seen (Fig. 2d). 30 min after incubation with both types of QDs, a part of the cells demonstrated a pronounced alteration, which could manifest as a destruction of the membrane (Fig. 2e) or the destruction of the membrane together with the cytoplasmic part (Fig. 2f), which indicates cell death by necrosis.

Thus, the following features of phagocytosis of QDs were established using the SEM method: (1) formation of «melting » areas on pseudopodia (Fig. 2b); (2) cell polarization (Fig. 2d); (3) formation of areas of the membrane destruction (Fig. 2e, f); (4) formation of large QD aggregates by cells and their concentration in the nucleus area (Fig. 2c, d, f). The latter phenomenon was also proved using the EDXMA (Fig. 4).

3.3. Proof of intracellular localization of QDs aggregates using the EDXMA

The EDXMA data directly prove the intracellular localization of CdSe/ZnS-MPA in the nucleus area (Fig. 4a), as indicated by the colocalization profile of cadmium (the main element of the QDs core) and sulfur (the main element of the QDs shell) (Fig. 4d, g). Similarly, the study of the spectrum of elements shows that the Cd/Se elements are found exclusively in the nucleus area (Fig. 4a, h, i), but not in the cytoplasmic part of the cell, where only traditional organic elements are present (Fig. 4a–f). It proves once again that the result of phagocytosis is the transfer of major aggregates to the perinuclear area of neutrophils.

https://doi.org/10.1016/j.heliyon.2019.e01439

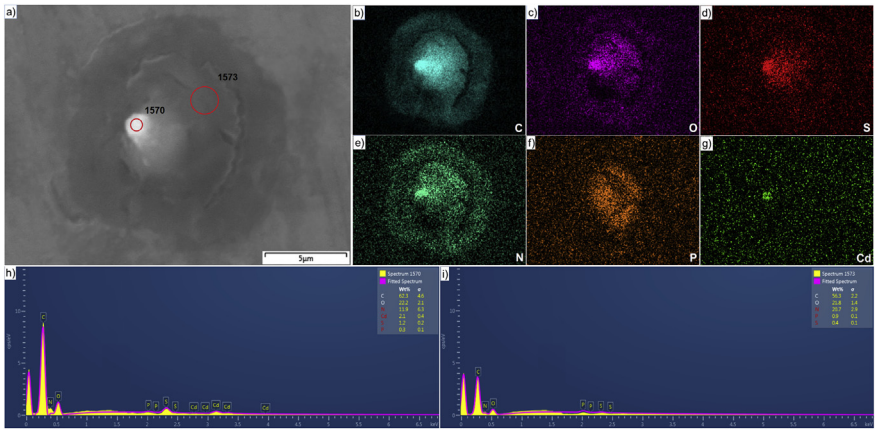

Fig. 4. EDXMA image of the neutrophil (a) and the map of distribution C (b), O (c), S (d), N (e), F (f), Cd (g), spectrum of elements in point 1570 (h), spectrum of elements in point 1573 (i).

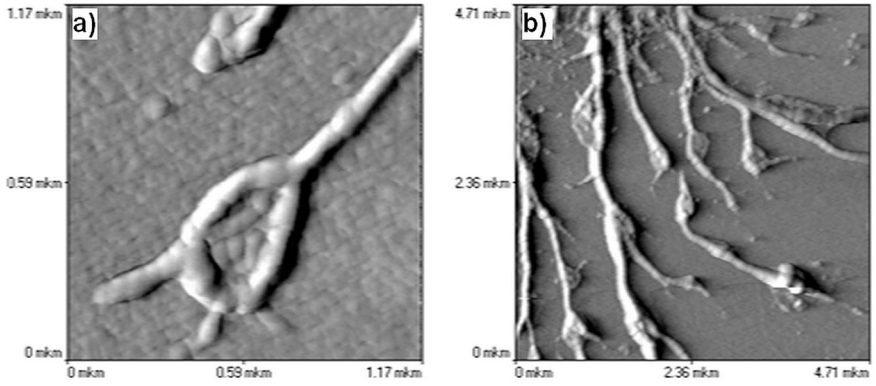

Fig. 5. «Melted » areas at the ends of pseudopodia formed after the contact with CdSe/ZnS-MPA (a); after the contact with CdSe/CdZnS/ZnS-PTVP (b).

3.4. Features of QD phagocytosis, investigated by AFM

On preparations fixed 15 min after the introduction of QDs, we observed formation of pseudopodia with «melted » ends (Fig. 5). Partial destruction of pseudopodia, arising from contact with QDs, is evident.

Alteration of pseudopodia is a phenomenon characteristic only of QDs (both types) and has never been encountered in the study of bacterial phagocytosis (Fig. 3 a, b). However, the destruction of individual pseudopodia is not the only process that occurs; the entire cell membrane also undergoes alteration (Fig. 6). It is obvious that the membrane thinning occurs due to the redistribution of cytoplasmic content, when swelling occurs around the nucleus (at the 30 min point, Figs. 6e, 6k), while the periphery is substantially thinned and a «crack» in the membrane appears (Fig. 6e), which grows quite rapidly and reaches large dimensions by 60 min (Fig. 6h). A similar damage to the membrane was observed by confocal microscopy (Fig. 9a) and the SEM (Fig. 2e). Thus, the alteration of membrane structures is observed

https://doi.org/10.1016/j.heliyon.2019.e01439

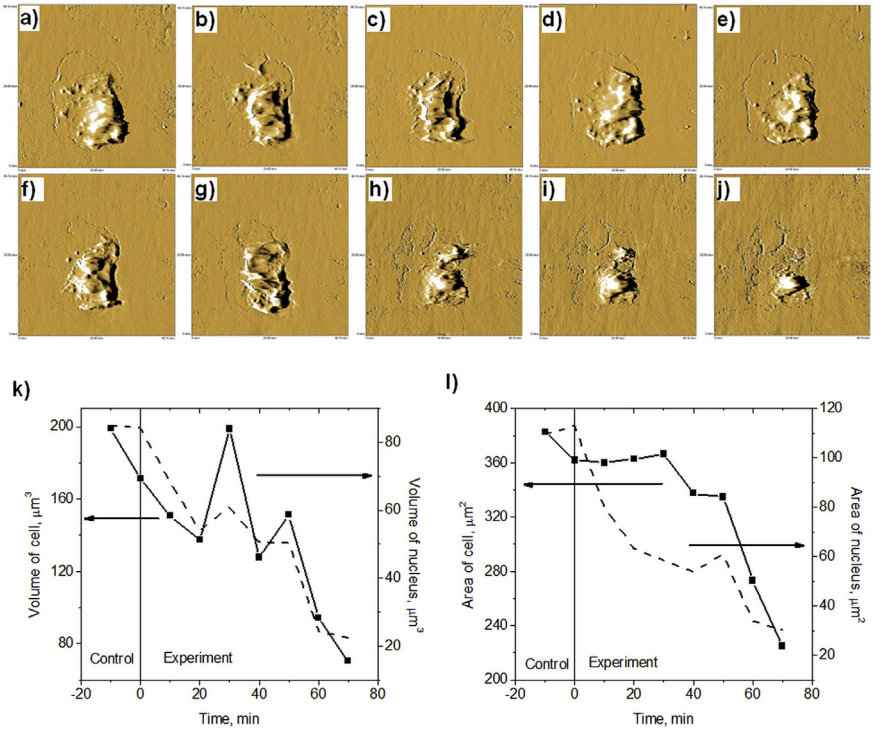

Fig. 6. Change in the basic morphometric characteristics of the neutrophil in the process of phagocytosis and cell death: control (a, b); time after the addition of CdSe/ZnS-MPA is indicated further: 10 min (c); 20 min (d); 30 min (e); 40 min (f); 50 min (g); 60 min (h); 70 min (i); 80 min (j); graph of changes in cell and nucleus volumes in the process of phagocytosis of CdSe/ZnS-MPA (k); graph of cell and nucleus area changes during the CdSe/ZnS-MPA phagocytosis (l).

already at the stage of QDs phagocytosis, even though the presence of granules in the cell is recorded up to 40 min (Fig. 6f). Changes in the morphometric parameters of the cell are shown in Figs. 6k and 6l. It is obvious that both the volume and the area of the cell decreased (the latter due to a rupture in the cytoplasm) as a result of CdSe/ZnS-MPA phagocytosis. In general, the volume of the cell decreases by 62%, the volume of the nucleus by 71%, the cell area by 38%, and the nucleus area by 70% in comparison to the control. Ultimately, the cell volume is determined only by the nucleus, which proves a rapid loss of fluid by the cell.

Figs. 7 and 8 demonstrate the results obtained during the study of phagocytosis of vital neutrophil granulocyte groups in dynamics, in the real time mode.

In the vital study of whole groups of neutrophil granulocytes, the following phenomenology is additionally revealed: (1) swelling of cells immediately after addition of QDs (Fig. 7b, Fig 8b); (2) clear contouring of the nucleus with the exit of the nucleus elements to the surface (Fig. 7b,c, Fig. 8b); (3) movement of cells toward each other, often with the formation of aggregates (Fig. 7c – h, Fig. 8b–f); (4) formation of a QDs halo around the periphery of cells (Fig. 7g–h, Fig. 9c); (5) thinning of the cell membrane along the periphery (in the cytoplasmic part of the cells) at the late stage

https://doi.org/10.1016/j.heliyon.2019.e01439

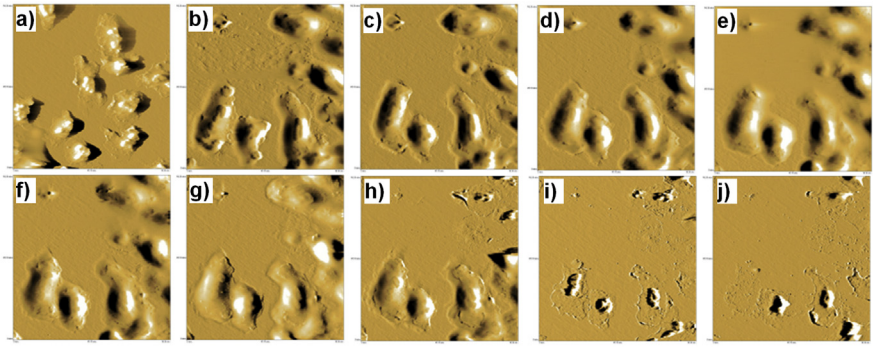

Fig. 7. Dynamics of changes in live neutrophil granulocytes in the process of CdSe/ZnS-MPA phagocytosis (0.025 mg/ml) studied in real time regime: (a) control, the time after the addition of QDs is indicated further, (b) 20 min; (c) 40 min; (d) 50 min; (e) 60 min; (f) 70 min; (g) 80 min; (h) 90 min; (i) 100 min; (j) 130 min.

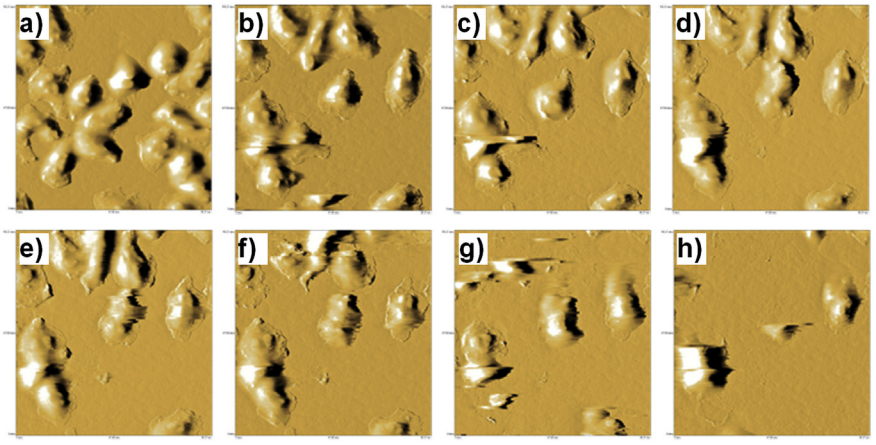

Fig. 8. Dynamics of changes in neutrophil granulocytes in the process of the CdSe/CdZnS/ZnS-PTVP phagocytosis (0.04 mg/ml) studied in real time on live neutrophils: (a) control, the time after the introduction of QDs is indicated further, (b) 10 min; (c) 20 min; (d) 30 min; (e) 45 min; (f) 50 min; (g) 60 min; (h) 70 min.

of incubation (100−130 min) (Fig. 7i−j); (6) transfer of QDs aggregates from cell to cell in case of close contacts between them (Fig. 8b−f).

Apparently, some of the neutrophils are able to act as a kind of «cells-distributors», which are capable of transmitting QDs aggregates to other cells (Fig. 8b−f). Accordingly, neutrophils accepting aggregates move toward these «cells-distributors».

In the study of QDs phagocytosis, cells demonstrate functional inhomogeneity, which manifests itself in different degrees of mobility and different phagocytic activity of neutrophils. However, the cells also have common features. These include swelling around the nucleus immediately after the beginning of interaction with QDs and the propensity to form aggregates. It should be noted that the cells swelling

https://doi.org/10.1016/j.heliyon.2019.e01439

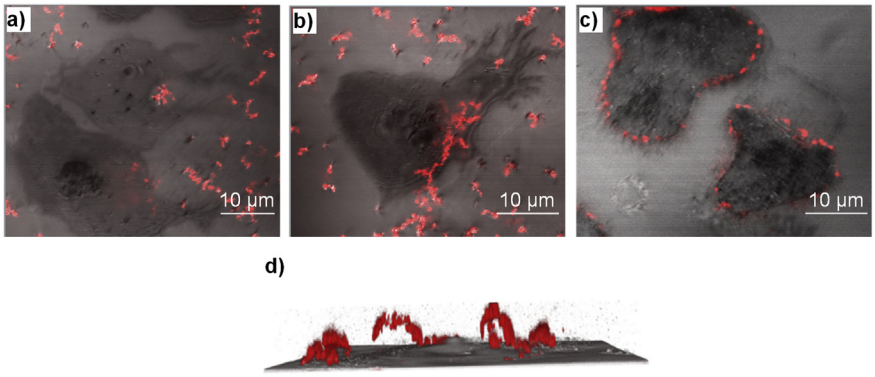

Fig. 9. Interaction of neutrophils with QDs. Video was captured by the Zeiss Axiovert 200M LSM 510 META confocal microscope with a ×100 magnification: phagosome formation to capture a large CdSe/CdZnS/ZnS-PTVP aggregates, movement of QDs from the periphery to the nucleus area (a); formation of pseudopodia by neutrophils, cells forming large aggregates of CdSe/CdZnS/ZnS-PTVP (b); QDs halos forming around dead neutrophil granulocytes according to the autophagic mechanism (c); formation of halos in a 3D image (d).

reaction is non-specific and was observed by us earlier, in response to other traumatic influences (non-optimal pH, excessive mechanical stimulus, etc.) (Pleskova et al., 2006).

3.5. Features of the QDs phagocytosis studied by confocal microscopy

The results of the study are shown in Fig. 9 and in the Appendix.

The confocal microscopy allows us to record the following phenomena of the QDs phagocytosis: (1) formation of large QDs aggregates by cells (Fig. 9a, b, Appendix); (2) transfer of QDs aggregates between cells (Appendix); (3) high chemotactic activity of neutrophils during this transfer (Appendix); (4) movement of QDs aggregates within cells with their concentration in the nucleus area (Fig. 9b, Appendix); (5) eventually, after cells death, formation of QDs halos around them (Fig. 9c—d, Appendix).

The perinuclear location of QDs was also observed in the work of Manshian et al. (2017). The authors attributed such a localization to the concentration of acidic lysosomes that perform QDs degradation processes in this region.

For QDs, the possibility of not simply capture by neutrophil, but also of trans-neutrophil transmission was noted for the first time. It is not yet clear for what reason neutrophil granulocytes transmit pre-aggregated QDs, however, in order to transmit or obtain these aggregates, the cells demonstrate sufficiently high chemotactic activity (Appendix). Most likely, QDs modulate this activity of neutrophils.

https://doi.org/10.1016/j.heliyon.2019.e01439

3.6. Changes in the biochemical profile of neutrophils after the QDs phagocytosis

The results of changes in the activity of NADPH oxidase, MPO and the CP level after the exposure to QDs are summarized in Table 1. Since the calculation of these enzymes activity was performed by an immunocytochemical method with the calculation of the average cytochemical coefficient, the results of the studies are expressed in arbitrary units (a.u.).

One of the main causes of the nanomaterials' toxicity is attributed to their ability to induce the formation of reactive oxygen species (ROS) (Li et al., 2010; Naqvi et al., 2010; Zhang et al., 2011; Ma et al., 2011; Chen et al., 2013). For neutrophils, this is of fundamental importance, since their production of ROS in the process of a respiratory burst is the molecular basis for cells to perform the effector function.

The results show that in neutrophils not activated by zymosan, QDs cause suppression of NADPH oxidase, while CdSe/CdZnS/ZnS-PTVP, which are more difficult to be phagocytosed by cells, cause a more pronounced suppression than CdSe/ZnS-MPA. This may be connected to the fact that the complex of NADPH oxidase is collected on the cytoplasmic membrane, so damage to the complex can occur both from the inner and the outer side of the membrane.

However, in cells primed with zymosan, incubation with QDs, on the contrary, causes a more pronounced respiratory burst compared to the control. Thus, at CL_{50} concentrations of QDs, neutrophils go into a hyperactivated state, as evidenced by a significant increase in AI cells. However, judging by the NFR growth, the reserve of the cell is sufficient to compensate for the effect of ROS hyperproduction. In addition to the superoxide-anion radical (O_2^-) and hydrogen peroxide (H_2O_2),

Table 1. Change in biochemical profile of neutrophils after quantum dots phagocytosis.

Enzymes	Control	CdSe/ZnS-MPA (0.025 mg/ml)	CdSe/CdZnS/ZnS-PTVP (0.04 mg/ml)
NBT_{sp}	0,99 ± 0,08 a.u. (n = 12)	0,94 ± 0,25* a.u. (n = 12; W = 66; Z = 2.08)	0,82 ± 0,24* a.u. (n = 12; W = 72; Z = 2.55)
NBT_{st}	1,19 ± 0,08 a.u. (n = 12)	1,61 ± 0,55* a.u. (n = 12; W = 12; Z = -2.07)	1,53 ± 0,29* a.u. (n = 12; W = 0; Z = - 3.02)
AI	1,20 ± 0,04 a.u. (n = 12)	1,69 ± 0,34* a.u. (n = 12; W = 0; Z = -3.02)	2,03 ± 0,74* a.u. (n = 12; W = 0; Z = - 3.02)
NFR	0,20 ± 0,03 a.u. (n = 12)	0,67 ± 0,37* a.u. (n = 12; W = 1; Z = -2.94)	0,72 ± 0,13* a.u. (n = 12; W = 0; Z = -3.02)
MPO	1,53 ± 0,17 a.u. (n = 12)	1,69 ± 0,4* a.u. (n = 12; W = 10; Z = - 2.01)	1,54 ± 0,28 a.u. (n = 12; W = 53; Z = 1.06)
CP	1,11 ± 0,3 a.u. (n = 12)	1,44 ± 0,22* a.u. (n = 12; W = 1; Z = - 2.8)	1,46 ± 0,32* a.u. (n = 12; W = 4; Z = - 2.7)

Note: * – differences with control are statistically significant ($p < 0.05$); NBT_{sp} – NADPH oxidase activity in a spontaneous test; NBT_{st} - NADPH oxidase activity in a stimulated test; n – number of studies.

https://doi.org/10.1016/j.heliyon.2019.e01439

which are formed when the NADPH-oxidase complex is activated, we can postulate the hyperproduction of hypochloric acid (HOCl) in the case of CdSe/ZnS-MPA, as we observed statistically significant differences between the activity of MPO in the control and after processing of neutrophils with CdSe/ZnS-MPA.

Since ROS are able to perform a regulatory function, it can be hypothesized that they can act as a driver for the process of transneutrophil transfer of QD aggregates.

Similarly, the study demonstrated the activation of oxygen-independent cell metabolism under the influence of QDs, as the level of CP increased significantly in comparison with the control.

Thus, in the process of phagocytosis, both types of QDs cause similar changes in the biochemical profile of neutrophils. Differences were observed only in the activity of MPO: the enzyme was activated under the influence of CdSe/ZnS-MPA, while under the influence of CdSe/CdZnS/ZnS-PTVP it remained at the control level. Thus, QDs caused activation of both oxygen-dependent and oxygen-independent metabolism of neutrophil granulocytes in the CL_{50}. In our previous studies, it was shown that lethal concentrations of the same types of QDs cause a dose-dependent suppression of neutrophil metabolism (Pleskova and Mikheeva, 2011). That means that under the influence of CL_{50} and other sublethal concentrations, QDs cause hyperactivation of cell metabolism, but NFR is sufficient to compensate for this hyperactivation, but as the concentration of nanomaterials increases, the compensatory mechanisms fail and the cells die.

4. Conclusion

Morphometric studies have made it possible to determine the features of the QDs phagocytosis by neutrophils. The main differences between the phagocytosis of nanomaterials and the bacterial phagocytosis are: alteration of cellular structures already in the early stages of phagocytosis (pseudopodia), redistribution of cytoplasmic content of the cell, formation of large aggregates of QDs and their transfer to the perinuclear area, aggregation of neutrophils and possibility of transneutrophil transmission of QDs. Metabolism of neutrophils also differs after the QDs phagocytosis. In particular, the inhibition of the NADPH-oxidase activity in non-primed neutrophils (activation is typical for bacteria) and cationic proteins activation (for bacteria, by contrast, inhibition is typical) were revealed. Thus, the phagocytosis of nanomaterials differs from the classical phagocytosis of bacteria according to the structural morphological and biochemical properties.

Both types of QDs, despite the different phagocytosis activity (CdSe/CdZnS/ZnS-PTVP are captured less actively), cause an identical change in the metabolism of neutrophils, besides the activity of MPO: the CdSe/ZnS-MPA phagocytosis induces enzyme activation, whereas the CdSe/CdZnS/ZnS-PTVP phagocytosis does not

https://doi.org/10.1016/j.heliyon.2019.e01439

change its activity in comparison with the control. It can be hypothesized that MPO activation is associated with some critical level of QDs uptake by the cell.

Declarations

Author contribution statement

S.N. Pleskova: Conceived and designed the experiments; Analyzed and interpreted the data; Wrote the paper.

R.N. Kriukov: Conceived and designed the experiments; Contributed reagents, materials, analysis tools or data.

E.N. Gorshkova: Conceived and designed the experiments; Performed the experiments; Analyzed and interpreted the data.

A.V. Boryakov: Conceived and designed the experiments; Analyzed and interpreted the data; Contributed reagents, materials, analysis tools or data.

Funding statement

This work was supported by a grant from the Russian Science Foundation, Project No. 16- 14-10179.

Competing interest statement

The authors declare no conflict of interest.

Additional information

Supplementary content related to this article has been published online at https://doi.org/10.1016/j.heliyon.2019.e01439.

Acknowledgements

The authors are sincerely grateful to Prof. Vodeneev V.A. and Balalaeva I.V. for the possibility of using a confocal microscope. The work was partially carried out using the equipment of the center for collective use of scientific equipment « New Materials and Resource-Saving Technologies».

References

Abdelmonem, A.M., Pelaz, B., Kantner, K., Bigall, N.C., Del Pino, P., Parak, W.J., 2015. Charge and agglomeration dependent in vitro uptake and cytotoxicity of zinc oxide nanoparticles. J. Inorg. Biochem. 153, 334−338.

Aguado, M.T., Pujol, N., Rubiol, E., Tura, M., Celada, A., 1980. Separation of granulocytes from peripheral blood in a single step using discontinuous density gradients of Ficoll-Urografin. A comparative study with separation by dextran. J. Immunol. Methods 32, 41–50.

Astaldi, G., Verga, L., 1957. The glycogen content of the cells of lymphatic leukaemia. Acta Haematol. 17 (3), 129–135.

Babin, K., Goncalves, D.M., Girard, D., 2015. Nanoparticles enhance the ability of human neutrophils to exert phagocytosis by a Syk-dependent mechanism. Biochim. Biophys. Acta 1850 (11), 2276–2282.

Bazarny, V.V., Tikhonina, E.N., Kondrashov, K.V., 2012. Determination of myeloperoxidase neutrophils in the surgical treatment of coronary heart disease. Clin. Lab. Diagnos. 7, 8–10.

Belyaeva, T.N., Salova, A.V., Leonteva, E.A., Mozhenok, T.M., Kornilova, E.S., Krolenko, S.A., 2009. Inappropriate quantum points in vital confocal microscopic examinations of cells. Tsitologiia 51 (10), 838–848.

Beste, M.T., Lomakina, E.B., Hammer, D.A., Waugh, R.E., 2015. Immobilized IL-8 triggers phagocytosis and dynamic changes in membrane microtopology in human neutrophils. Ann. Biomed. Eng. 43 (9), 2207–2219.

Chen, Q., Xue, Y., Sun, J., 2013. Kupffer cell-mediated hepatic injury induced by silica nanoparticles in vitro and in vivo. Int. J. Nanomed. 8, 1129–1140.

Crane, J.M., Haggie, P.M., Verkman, A.S., 2009. Quantum dot single molecule tracking reveals a wide range of diffusive motions of membrane transport proteins. Proc. SPIE 7489, 71890Y. (1-10).

Fine, N., Barzilay, O., Glogauer, M., 2017. Analysis of human and mouse neutrophil phagocytosis by flow cytometry. Methods Mol. Biol. 1519, 17–24.

Gao, X., Cui, Y., Levenson, R.M., Chung, L.W., Nie, S., 2004. In vivo cancer targeting and imaging with semiconductor quantum dots. Nat. Biotechnol. 22 (8), 969–976.

Gatto, F., Cagliani, R., Catelani, T., Guarnieri, D., Moglianetti, M., Pompa, P.P., Bardi, G., 2017. PMA-induced THP-1 macrophage differentiation is not impaired by citrate-coated platinum nanoparticles. Nanomaterials (Basel) 7, 332. (1-10).

Guo, Z., Tan, L., 2009. Fundamentals and Applications of Nanomaterials. Artech House, London, 249p.

Hanaki, K., Momo, A., Oku, T., Komoto, A., Maenosono, S., Yamaguchi, Y., Yamamoto, K., 2003. Semiconductor quantum dot/albumin complex is a long-

https://doi.org/10.1016/j.heliyon.2019.e01439

life and highly photostable endosome marker. Biochem. Biophys. Res. Commun. 302, 496−501.

Kaplow, L.S., 1995. A histochemical procedure for localizing and evaluating leukocyte alkaline phosphatase activity in smears of blood and marrow. Blood 10 (10), 1023−1029.

Kim, S., Lim, Y.T., Soltesz, E.G., De Grand, A.M., Lee, J., Nakayama, A., Parker, J.A., Mihaljevic, T., Laurence, R.G., Dor, D.M., Cohn, L.H., Bawendi, M.G., Frangioni, J.V., 2004. Near-infrared fluorescent type II quantum dots for sentinel lymph node mapping. Nat. Biotechnol. 22 (1), 93−97.

Li, J.J., Hartono, D., Ong, C., Bay, B., Yung, L.L., 2010. Autophagy and oxidative stress associated with gold nanoparticles. Biomaterials 31 (23), 5996−6003.

Lidke, D.S., Nagy, P., Heintzmann, R., Arndt-Jovin, D.J., Post, J.N., Grecco, H.E., Jares-Erijman, E.A., Jovin, T.M., 2004. Quantum dot ligands provide new insights into erbB/HER receptor-mediated signal transduction. Nat. Biotechnol. 22 (2), 198−203.

Lim, Y.T., Kim, S., Nakayama, A., Stott, N.E., Bawendi, M.G., Frangioni, J.V., 2003. Selection of quantum dot wavelengths for biomedical assays and imaging. Mol. Imag. 2 (1), 50−64.

Liu, X., Zhu, H., Jin, Q., Zhou, W., Colvin, V.L., Ji, J., 2013. Small and stable phosphorylcholine zwitterionic quantum dots for weak nonspecific phagocytosis and effective Tat peptide functionalization. Adv. Healthc. Mater. 2 (2), 352−360.

Ma, J.Y., Zhao, H., Mercer, R.R., Barger, M., Rao, M., Meighan, T., Schwegler-Berry, D., Castranova, V., Ma, J.K., 2011. Cerium oxide nanoparticle-induced pulmonary inflammation and alveolar macrophage functional change in rats. Nanotoxicology 5 (3), 312−325.

Manshian, B.B., Martens, T.F., Kantner, K., Braeckmans, K., De Smedt, S.C., Demeester, J., Jenkins, G.J.S., Parak, W.J., Pelaz, B., Doak, S.H., Himmelreich, U., Soenen, S.J., 2017. The role of intracellular trafficking of CdSe/ZnS QDs on their consequent toxicity profile. J. Nanobiotechnol. 15, 45. (1-14).

Mayansky, A.N., Pikusa, O.I., 1993. The Clinical Aspects of Phagocytosis. Magarif, Kazan, 190p.

Musihin, S.F., Alexandrova, O.A., Luchinin, V.V., Maksimov, A.I., Moshnikov, V.A., 2012. Semiconductor colloidal nanoparticles in biology and medicine. J. Basic Biomed. Eng. 5−6, 47−55.

https://doi.org/10.1016/j.heliyon.2019.e01439

Naqvi, S., Samim, M., Abdin, M., Ahmed, F.J., Maitra, A., Prashant, C., Dinda, A.K., 2010. Concentration-dependent toxicity of iron oxide nanoparticles mediated by increased oxidative stress. Int. J. Nanomed. 5 (1), 983–989.

Nordenfelt, P., Tapper, H., 2011. Phagosome dynamics during phagocytosis by neutrophils. J. Leukoc. Biol. 90 (2), 271–284.

Nüsse, O., 2011. Biochemistry of the phagosome: the challenge to study a transient organelle. ScientificWorldJournal 11, 2364–2381.

Oberdörster, G., Stone, V., Donaldson, K., 2007. Toxicology of nanoparticles: a historical perspective. Nanotoxicology 1 (1), 2–25.

Pigarevskiy, V.E., 1988. Clinical Morphology of Neutrophil Granulocytes. Nauka, Leningrad, 139p.

Pleskova, S.N., Balalayeva, I.V., Gushchina, Y.Y., Sergeyeva, E.A., Zdobnova, T.A., Deev, S.M., Turchin, I.V., 2009. Distinctions in functional activity of neutrophilic granulocytes in reactions with semiconductor quantum dots. Morphology 135 (3), 47–49.

Pleskova, S.N., Gushchina, Yu.Yu., Zvonkova, M.B., Khomutov, A.E., 2006. Study of morphology and rigidity of neutrophil granulocyte membrane in the real time mode by scanning probe microscopy. Bull. Exp. Biol. Med. 141 (6), 712–715.

Pleskova, S.N., Kriukov, R.N., Razumkova, E.V., Zubkov, S.Yu., Abarbanel, N.V., 2018a. Features of opsonized and nonopsonized bacteria S.aureus and E.coli which are phagocyted by human neutrophil granulocytes, studied by atomic force microscopy Cytology. Cell Tissue Biol. 60 (8), 623–631.

Pleskova, S.N., Mikheeva, E.R., 2011. Modulation of oxygen-dependent and oxygen-independent metabolism of neutrophil granulocytes by quantum dots. Bull. Exp. Biol. Med. 151 (4), 452–454.

Pleskova, S.N., Mikheeva, E.R., Gornostaeva, E.E., 2018b. The interaction between human blood neutrophil granulocytes and quantum dots. Micron 105, 82–92.

Pleskova, S.N., Zvonkova, M.B., Gushchina, Yu.Yu., 2005. Scanning probe microscopy for the study of morphological parameters of neutrophil granulocytes. Morphology 127, 60–62.

Rabinovitch, M., 1995. Professional and non-professional phagocytes: an introduction. Trends Cell Biol. 5, 85–87.

Rhyner, M.N., Smith, A.M., Gao, X., Mao, H., Yang, L., Nie, S., 2006. Quantum dots and multifunctional nanoparticles: new contrast agents for tumor imaging. Nanomedicine 1 (2), 209–217.

https://doi.org/10.1016/j.heliyon.2019.e01439

Sakai, J., Li, J., Subramanian, K.K., Mondal, S., Bajrami, B., Hattori, H., Jia, Y., Dickinson, B.C., Zhong, J., Ye, K., Chang, C.J., Ho, Y.S., Zhou, J., Luo, H.R., 2012. Reactive oxygen species-induced actin glutathionylation controls actin dynamics in neutrophils. Immunity 37 (6), 1037−1049.

Uribe-Querol, E., Rosales, C., 2017. Control of phagocytosis by microbial pathogens. Front. Immunol. 8, 1368. (1-23).

Wu, X., Liu, H., Liu, J., Haley, K.N., Treadway, J.A., Larson, J.P., Ge, N., Peale, F., Bruchez, M.P., 2002. Immunofluorescent labeling of cancer marker Her2 and other cellular targets with semiconductor quantum dots. Nat. Biotechnol. 21 (1), 41−46.

Xie, Y., Wan, B., Yang, Y., Cui, X., Xin, Y., Guo, L.H., 2019. Cytotoxicity and autophagy induction by graphene quantum dots with different functional groups. J. Environ. Sci. (China). 77, 198−209.

Xing, Y., Chaudry, Q., Shen, C., Kong, K.Y., Zhau, H.E., Chung, L.W., Petros, J.A., O'Regan, R.M., Yezhelyev, M.V., Simons, J.W., Wang, M.D., Nie, S., 2007. Bioconjugated quantum dots for multiplexed and quantitative immunohistochemistry. Nat. Protoc. 2 (5), 1152−1165.

Xu, L., Dai, Y., Wang, Z., Zhao, J., Li, F., White, J.C., Xing, B., 2018. Graphene quantum dots in alveolar macrophage: uptake-exocytosis, accumulation in nuclei, nuclear responses and DNA cleavage. Part. Fibre Toxicol. 15 (1), 45. (1-17).

Yashin, K.D., Osipovich, V.D., Pitsuk, S.E., 2007. Structure of the nanocrystals of cadmium selenit received by the method of colloid chemistry for the use in medical diagnostics. Rep BGUIR 3, 74−79.

Zhang, X.Q., Yin, L.H., Tang, M., Pu, Y.P., 2011. ZnO, TiO2, SiO2, and Al2O3 nanoparticles-induced toxic effects on human fetal lung fibroblasts. Biomed. Environ. Sci. 24 (6), 661−669.

https://doi.org/10.1016/j.heliyon.2019.e01439